Observation of Ultrastrong Spin-Motion Coupling for Cold Atoms in Optical Microtraps

A. Dareau,[1] Y. Meng,[1] P. Schneeweiss,[1,*] and A. Rauschenbeutel[1,2,†]
[1]Vienna Center for Quantum Science and Technology, TU Wien—Atominstitut, Stadionallee 2, 1020 Vienna, Austria
[2]Department of Physics, Humboldt-Universität zu Berlin, 10099 Berlin, Germany

(Received 11 September 2018; revised manuscript received 18 November 2018; published 21 December 2018)

We realize a mechanical analogue of the Dicke model, achieved by coupling the spin of individual neutral atoms to their quantized motion in an optical trapping potential. The atomic spin states play the role of the electronic states of the atomic ensemble considered in the Dicke model, and the in-trap motional states of the atoms correspond to the states of the electromagnetic field mode. The coupling between spin and motion is induced by an inherent polarization gradient of the trapping light fields, which leads to a spatially varying vector light shift. We experimentally show that our system reaches the ultrastrong coupling regime; i.e., we obtain a coupling strength that is a significant fraction of the trap frequency. Moreover, with the help of an additional light field, we demonstrate the *in situ* tuning of the coupling strength. Beyond its fundamental interest, the demonstrated one-to-one mapping between the physics of optically trapped cold atoms and the Dicke model paves the way for implementing protocols and applications that exploit extreme coupling strengths.

DOI: 10.1103/PhysRevLett.121.253603

The quantum Rabi model (QRM) describes the interaction of a two-level emitter with a single quantized mode of the electromagnetic field. Together with its extension for an ensemble of emitters, i.e., the Dicke model (DM), it constitutes a cornerstone of quantum optics [1]. The physics predicted by the QRM and the DM strongly depends on the relative values of the mode frequency ω and the coupling strength between the two-level system (TLS) and the bosonic mode g. For weak coupling, i.e., $g/\omega \ll 1$, the rotating wave approximation (RWA) applies. In this case, the QRM and the DM reduce to the Jaynes-Cummings and the Tavis-Cummings models, respectively. The RWA breaks down in the ultrastrong coupling regime (USC), i.e., for $g/\omega \gtrsim 0.1$. When increasing the coupling strength further, one enters the deep-strong coupling regime (DSC) [2]. For such high values of g/ω, new phenomena are expected [3–7]. The existence of a quantum phase transition in the thermodynamic limit adds to the richness of the DM [8–10]. Furthermore, USC and DSC may enable novel protocols for quantum communication and quantum information processing [11–13].

Over the last decade, USC was reached using various experimental platforms [14–22]. More recently, DSC was achieved in circuit quantum electrodynamics [23,24] as well as by coupling a THz metamaterial with cyclotron resonances in a two-dimensional electron gas [25]. While these systems reach record-high ratios of g/ω, the large coupling strengths make state preparation and readout challenging. For this reason, alternative routes were proposed to achieve large coupling in experimental platforms that, at the same time, offer a high level of control and tunability. Following this path, the QRM in the USC and DSC regimes was simulated using circuit quantum electrodynamics [26,27], and DSC was studied with single trapped ions [28].

Here, we implement a mechanical analogue of the Dicke model by coupling the spin of individual neutral atoms to their quantized motion in a trapping potential. In our approach, the coupling is enabled by spatial gradients of the vector light shift inherent to optical microtraps. Fluorescence spectroscopy, which was recently used to measure the temperature of atoms in a nanofiber-based trap after degenerate Raman cooling [29], grants access to the energy spectrum of the system. We observe vacuum Rabi splittings and transitions between dressed states that both clearly and consistently reveal an ultrastrong spin-motion coupling in our experiment; i.e., the coupling strength is a significant fraction of the mode frequency. Furthermore, we demonstrate that the coupling strength can be readily tuned *in situ* using an additional laser light field.

Our implementation employs laser-cooled individual cesium atoms trapped in the evanescent light field surrounding the nanofiber section of a tapered optical fiber, see Fig. 1(a) and the Supplemental Material [30]. The strong transverse confinement of the trapping light fields results in a strong polarization gradient in the azimuthal direction. In addition to the scalar light shift that gives rise to trapping, atoms in the evanescent field then experience a spatially varying vector light shift [29,35]. This shift can be thought of as arising from the Zeeman interaction with a position-dependent fictitious magnetic field, $\boldsymbol{B}_{\mathrm{fict}}$ [36]. For our configuration, $\boldsymbol{B}_{\mathrm{fict}}$ mainly points along the x direction, see Fig. 1(b). Near the trap minimum, the x component of the fictitious magnetic field varies approximately linearly along y, so that $\boldsymbol{B}_{\mathrm{fict}} \approx b_y y \boldsymbol{e}_x$, with $\boldsymbol{e}_x$ the unit vector along x and $b_y \approx 1.9\ \mathrm{G}/\mu\mathrm{m}$.

The Zeeman interaction of a trapped atom with this fictitious magnetic field results in a coupling between the atomic spin and motional degrees of freedom (DOF). Here,

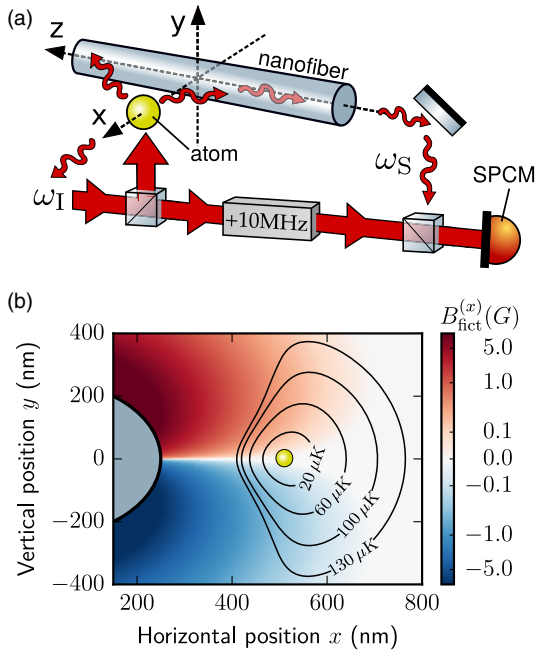

FIG. 1. Experimental setup. (a) Individual cesium atoms are trapped near the surface of an optical nanofiber. They are exposed to a near-resonant excitation laser field (frequency $\omega_{\rm I}$), propagating along the $+y$ direction. A fraction of the atomic fluorescence is scattered into the guided mode of the nanofiber (frequency $\omega_{\rm S}$). This light is superposed with a reference beam that is derived from the excitation laser and frequency shifted by $+10$ MHz. The resulting beat note is recorded with a single photon counting module (SPCM). Its Fourier analysis yields the fluorescence spectrum, which grants access to the energy spectrum of the trapped atoms. (b) Contours of the scalar part of the trapping potential (black lines). The yellow dot marks the position of the atom at the trap minimum. The trapping light fields also give rise to a spatially varying fictitious magnetic field (main component $B^{(x)}_{\rm fict}$ shown in density plot) that couples the atomic spin and its motional DOF.

we assume a harmonic trapping potential, with a set of frequencies $\{\omega_i\}$ and annihilation operators $\{\hat{a}_i\}$ $(i = x, y, z)$. In addition to $\boldsymbol{B}_{\rm fict}$, we apply a homogeneous offset magnetic field, $\boldsymbol{B}_0 = B_0\boldsymbol{e}_y$, along the y direction. The dynamics of a trapped atom is then described by the following Hamiltonian:

$$\hat{H} = \sum_{i=x,y,z} \hbar\omega_i \hat{a}_i^\dagger \hat{a}_i + g_F \mu_B \hat{\boldsymbol{F}} \cdot (\boldsymbol{B}_0 + \boldsymbol{B}_{\rm fict}), \qquad (1)$$

with g_F the hyperfine Landé factor and μ_B the Bohr magneton. Assuming that the fictitious magnetic field consists of a linear gradient along y, and only considering the y motional DOF, we can rewrite Eq. (1) as [30]

$$\hat{H}_y = \hbar\omega_y \hat{a}_y^\dagger \hat{a}_y + \hbar\Delta \hat{F}_y + \frac{\hbar g_y}{\sqrt{2F}}(\hat{a}_y^\dagger + \hat{a}_y)(\hat{F}_+ + \hat{F}_-), \qquad (2)$$

where $\hat{F}_+$ ($\hat{F}_-$) is the spin raising (lowering) operator for the eigenstates of $\hat{F}_y$ with eigenvalues $\hbar m_F$. For $F = 1/2$, Hamiltonian (2) corresponds to the QRM, while for $F > 1/2$, as is the case for cesium, it corresponds to the DM. The physics is governed by three parameters: The mode frequency ω_y, the Zeeman splitting between adjacent m_F states $\Delta \propto B_0$, and the spin-motion coupling strength $g_y \propto b_y$. For our configuration, we expect $g_y \approx 2\pi \times 19$ kHz for a calculated trap frequency $\omega_y \approx 2\pi \times 95$ kHz, i.e., $g_y/\omega_y \approx 0.2$.

The low-energy eigenstates of $\hat{H}_y$ are illustrated in Figs. 2(a), 2(b). We consider the case of cesium in the $F = 4$ hyperfine ground state. In the absence of spin-motion coupling ($g_y = 0$), the eigenstates are the bare states $|m_F, n_y\rangle$, where n_y corresponds to a Fock state of the harmonic trapping potential. In the presence of spin-motion coupling, the new eigenstates are dressed states. When the coupling is resonant ($\Delta = \omega_y$), the degeneracy of the bare states $|-4, 1\rangle$ and $|-3, 0\rangle$ is lifted, and the new eigenstates are $|\pm\rangle = (|-4, 1\rangle \mp |-3, 0\rangle)/\sqrt{2}$, separated in energy by $\hbar\Omega_y$, where $\Omega_y > 0$ is the Rabi frequency. Here, we expect $\Omega_y = 2g_y \approx 2\pi \times 38$ kHz [30].

In order to probe the low-energy part of Hamiltonian (2), we perform a heterodyne fluorescence spectroscopy measurement [29,37]. The experimental setup is sketched in Fig. 1(a). The atoms are exposed to a laser field propagating along the $+y$ axis and σ^--polarized with respect to the propagation direction. The laser is red detuned with respect to the cycling transition of the D_2 line of cesium, and its intensity is kept low enough to ensure that it is scattered coherently by the atoms. This laser provides degenerate Raman cooling [29] and optical pumping, so that most of the atoms populate the low-lying energy states depicted in Figs. 2(a), 2(b). Part of the fluorescence light is scattered into the guided mode of the optical nanofiber [38]. This light is superposed with a reference beam, derived from the excitation laser, and frequency shifted by $+10$ MHz. The resulting beat note is recorded using a single photon counting module (SPCM). Postprocessing of the SPCM data yields the intensity power spectral density (PSD). This heterodyne setup enables a precise measurement of the frequency difference between the incoming photons from the excitation beam (frequency ω_I) and the photons scattered by the atoms (frequency ω_S). In the case of elastic scattering, the atomic state and the frequency of the photons are unchanged ($\omega_I = \omega_S$), yielding the carrier peak in the PSD. In the case of inelastic scattering, the atomic state is changed and the difference of energy between the incoming and scattered photons has to match the difference of energy between the initial and final atomic states. This gives rise to sidebands around the carrier peak, the positions of which grant access to the energy spectrum of the atoms.

We record fluorescence spectra for different values of the Zeeman splitting, $\Delta \propto B_0$, see Figs. 2(c)–2(e). Far from resonance, i.e., for $|\Delta - \omega_i| \gg \Omega_i$, transitions between the

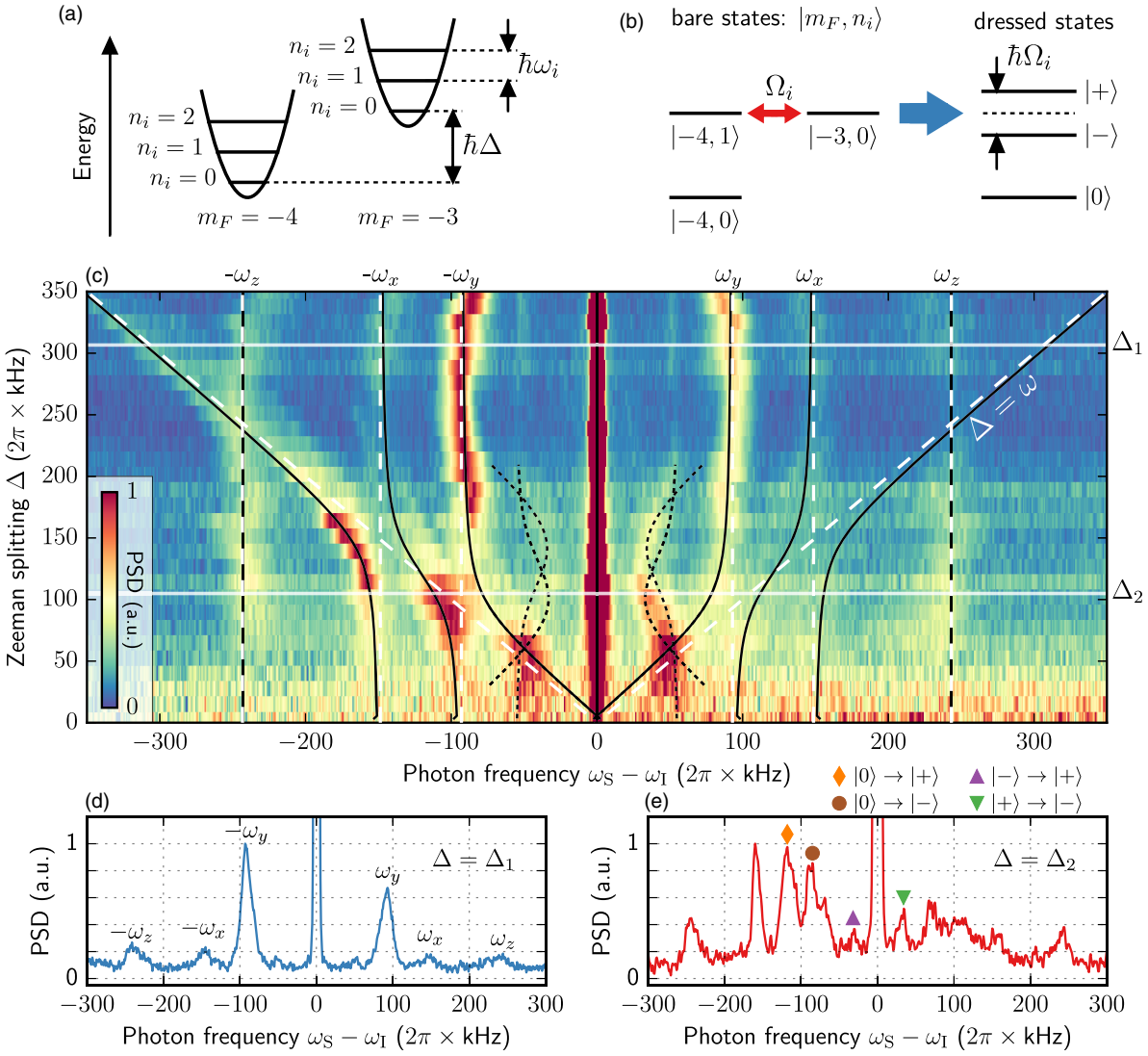

FIG. 2. Experimental signature of ultrastrong spin-motion coupling. (a) The bare eigenstates in the harmonic trapping potential are $|m_F, n_i\rangle$ with eigenenergies $\hbar(m_F\Delta + n_i\omega_i)$, where $\hbar\Delta$ is the Zeeman splitting between two neighboring m_F states and $\hbar\omega_i$ is the energy of one motional quantum. The spin-motion coupling is resonant for $\Delta = \omega_i$. (b) At resonance, the spin-motion coupling lifts the degeneracy between the bare states $|-4, 1\rangle$ and $|-3, 0\rangle$, and the new eigenstates $|+\rangle$ and $|-\rangle$ are split by $\hbar\Omega_i$. (c) Fluorescence spectra for different values of Δ. Avoided crossings occur when the resonance condition is fulfilled for the x and y DOF. Dashed white lines: predicted ground-to-bare state transitions derived from a fit of the data far from resonance. Solid black lines: ground-to-dressed state transitions with coupling strengths derived from a fit at resonance (see main text and [30]). Dashed black lines: interdressed state transitions. (d),(e), Fluorescence spectra, measured for two Zeeman splittings, Δ_1 and Δ_2, respectively [cf. solid horizontal white lines in (c)]. Far from resonance (d), three pairs of motional sidebands are apparent. When the coupling is resonant (e), one motional sideband is split. We also observe sidebands corresponding to transitions between the excited states.

bare states result in three pairs of motional sidebands; see Fig. 2(d). These transitions change the motional state of the atom but not its spin. These sidebands do not depend on Δ, and their positions can be used to infer the trap frequencies. We find $\{\omega_x,\omega_y,\omega_z\} = 2\pi \times \{149(2), 93(2), 243(5)\}$ kHz. The strong asymmetry of the amplitudes of the positive- and negative-frequency peaks indicates that the atoms are close to the motional ground state [29]. A fourth peak is also visible in the upper left part of Fig. 2(c). It corresponds to a transition between adjacent m_F states for a given motional state. Its position depends linearly on Δ. Close to resonance, we observe a splitting of the motional sideband corresponding to the resonantly coupled DOF. This is clearly visible in Fig. 2(e), which is measured close to the resonance of the y DOF. The width of the splitting already indicates that we operate in the USC regime. When scanning Δ around resonance, an avoided crossing is observed. Such an avoided crossing is also visible for the x DOF, indicating that strong spin-motion coupling is present for this DOF, too. This additional coupling could

arise from the polarizations of the trapping light fields not being perfectly aligned and/or from a spurious vector light shift originating from the interference of the probe light with its reflection on the nanofiber.

Besides the Rabi splitting, a new pair of peaks is apparent close to resonance. These sidebands, labeled by triangles in Fig. 2(e), are located at $\pm\Omega_i$ around the carrier and correspond to transitions between the dressed states. The observation of transitions from the ground state to the lowest pair of dressed states (vacuum Rabi splitting) and the simultaneous observation of transitions between the dressed states is enabled by two features of our system: First, although we achieve cooling close to the motional ground state [29], there is a finite population of the first excited states and, therefore, we can observe transitions starting from these states; second, the energy gap $\hbar\Omega_i$ between the dressed states is comparable to the energy gap between the ground state and the first excited state manifold $\hbar\omega_i$, so that the corresponding transitions have similar energy and can be detected by the same method. The position of these sidebands allows us to precisely measure the Rabi splitting Ω_i. We find $\Omega_y = 2\pi \times 35(1)$ and $\Omega_x = 2\pi \times 36(1)$ kHz. This corresponds to coupling strengths of $g_y/\omega_y = 0.19(1)$ and $g_x/\omega_x = 0.12(1)$, respectively. Thus, we clearly reach the ultrastrong coupling regime for both DOF [39].

Another feature of our setup is the possibility to tune the coupling strength *in situ*. For this purpose, we use an additional fiber-guided light field at the so-called tune-out wavelength [40] near 880 nm. At this wavelength, the scalar polarizability vanishes, so that this laser field only induces a vector light shift. This field propagates in the same direction as the blue-detuned trapping light field and has the same polarization. For this configuration, we expect a partial compensation of the fictitious magnetic field gradient [35] and, thus, a reduction of the coupling strength. To quantify this effect, we measured the Rabi splitting Ω_y, for different powers of the tune-out laser P_{880}; see Fig. 3. As expected in our regime, Ω_y decreases linearly with P_{880}. The measured slope is $d\Omega_y/dP_{880} = -120(10)$ Hz/μW. From an *ab initio* calculation, taking into account the vector polarizability of cesium and the mode function of the nanofiber-guided tune-out light, we expect -100 Hz/μW, in reasonable agreement with the experimental value. While the measurements reported in the present work can be explained in the framework of the RWA, increasing the coupling strength further should enable the observation of beyond-RWA effects [6,7], such as a deviation from the linear dependence of the Rabi splitting on the coupling strength. By changing its propagation direction, the tune-out laser field may indeed be used to enhance the coupling strength. In this case, a power of $P_{880} \approx 800$ μW should be sufficient to induce a coupling strength of about the trap frequency. By modulating the tune-out laser field intensity, one may dynamically adjust

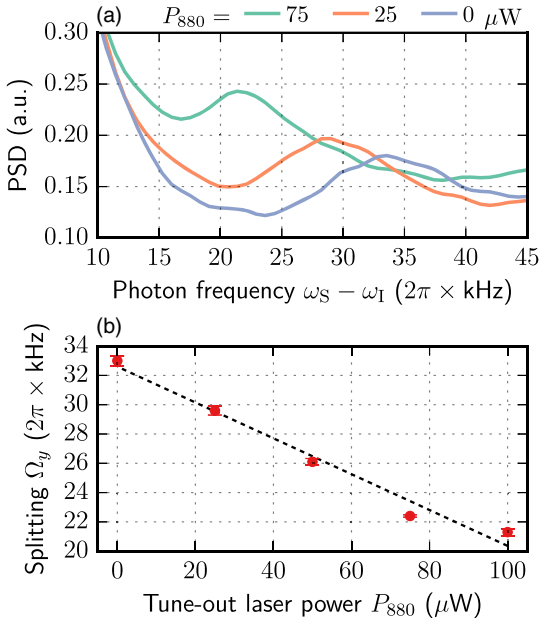

FIG. 3. Tunability of the spin-motion coupling strength. A nanofiber-guided tune-out laser field at a wavelength of $\lambda = 880$ nm allows one to modify the fictitious magnetic field gradient along y and, thus, the corresponding spin-motion coupling strength. (a) Fluorescence spectra, taken for resonant coupling of the y DOF ($\Delta = \omega_y$) and different values of the tune-out laser power, P_{880}. We show the data corresponding to the $|+\rangle \rightarrow |-\rangle$ interdressed state transition. The peak position corresponds to the Rabi splitting, Ω_y. It shifts towards the carrier for increasing values of P_{880}, indicating a reduction of the coupling strength. (b) As expected, the measured Ω_y (red dots) depends linearly on P_{880}. A fit (black dashed line) yields $d\Omega_y/dP_{880} = -120(10)$ Hz/μW. For $P_{880} > 100$ μW, the proximity of the carrier impedes a precise measurement of the peak position.

the coupling strength, even on timescales shorter than the Rabi oscillation period. This might enable, e.g., adiabatic USC/DSC ground-state preparation or the study of quench dynamics.

In summary, the demonstrated implementation of a mechanical analogue of the Dicke model with cold atoms constitutes a novel route to explore ultrastrong and, potentially, even deep-strong coupling phenomena with unprecedented level of control. Our approach is not restricted to nanofiber-based optical traps but can, e.g., also be implemented with atoms in an optical lattice [41] or in free-space optical microtraps [42,43]. In order to obtain a large spin-motion coupling strength, the vector light shift should vary significantly over the extent of the ground state center-of-mass wave function of a trapped atom [44]. Taking advantage of the rich toolbox developed in cold-atom physics, other techniques could be used in order to precisely probe the state of the motional DOF [35,45,46] and the spin DOF [47,48]. In this context, the ability to switch the spin-motion coupling off nonadiabatically is essential for projecting the system onto the uncoupled basis prior to detection.

Possible future research directions include the study of the dynamical Casimir effect via a modulation of the system parameters [49] or of the role of dissipation in the USC/DSC regime [50]. Understanding these effects will be beneficial, e.g., for the realization of ultrafast quantum gates [12,13] or of qubit protection protocols [11] relying on USC. Finally, a suitably tailored real and fictitious magnetic field pattern can be used to realize generalizations of the quantum Rabi model or of the Dicke model, such as the driven QRM, or to implement ultrastrong two-photon coupling [44].

Financial support by the European Research Council (CoG NanoQuaNt) and the Austrian Science Fund (FWF, SFB NextLite Project No. F 4908-N23 and DK CoQuS Project No. W 1210-N16) is gratefully acknowledged.

*philipp.schneeweiss@tuwien.ac.at
†arno.rauschenbeutel@hu-berlin.de

[1] D. Braak, Q.-H. Chen, M. T. Batchelor, and E. Solano, J. Phys. A **49**, 300301 (2016).
[2] D. Z. Rossatto, C. J. Villas-Bôas, M. Sanz, and E. Solano, Phys. Rev. A **96**, 013849 (2017).
[3] S. Ashhab and F. Nori, Phys. Rev. A **81**, 042311 (2010).
[4] J. Casanova, G. Romero, I. Lizuain, J. J. García-Ripoll, and E. Solano, Phys. Rev. Lett. **105**, 263603 (2010).
[5] L. Garziano, V. Macrì, R. Stassi, O. Di Stefano, F. Nori, and S. Savasta, Phys. Rev. Lett. **117**, 043601 (2016).
[6] P. Forn-Díaz, L. Lamata, E. Rico, J. Kono, and E. Solano, arXiv:1804.09275.
[7] A. F. Kockum, A. Miranowicz, S. De Liberato, S. Savasta, and F. Nori, arXiv:1807.11636.
[8] K. Hepp and E. H. Lieb, Ann. Phys. (N.Y.) **76**, 360 (1973).
[9] Y. K. Wang and F. T. Hioe, Phys. Rev. A **7**, 831 (1973).
[10] C. Emary and T. Brandes, Phys. Rev. Lett. **90**, 044101 (2003).
[11] P. Nataf and C. Ciuti, Phys. Rev. Lett. **107**, 190402 (2011).
[12] G. Romero, D. Ballester, Y. M. Wang, V. Scarani, and E. Solano, Phys. Rev. Lett. **108**, 120501 (2012).
[13] T. H. Kyaw, S. Felicetti, G. Romero, E. Solano, and L.-C. Kwek, Sci. Rep. **5**, 8621 (2015).
[14] A. A. Anappara, S. De Liberato, A. Tredicucci, C. Ciuti, G. Biasiol, L. Sorba, and F. Beltram, Phys. Rev. B **79**, 201303 (2009).
[15] G. Günter, A. A. Anappara, J. Hees, A. Sell, G. Biasiol, L. Sorba, S. De Liberato, C. Ciuti, A. Tredicucci, A. Leitenstorfer *et al.*, Nature (London) **458**, 178 (2009).
[16] J. Bourassa, J. M. Gambetta, A. A. Abdumalikov, O. Astafiev, Y. Nakamura, and A. Blais, Phys. Rev. A **80**, 032109 (2009).
[17] Y. Todorov, A. M. Andrews, R. Colombelli, S. De Liberato, C. Ciuti, P. Klang, G. Strasser, and C. Sirtori, Phys. Rev. Lett. **105**, 196402 (2010).
[18] T. Niemczyk, F. Deppe, H. Huebl, E. Menzel, F. Hocke, M. Schwarz, J. Garcia-Ripoll, D. Zueco, T. Hümmer, E. Solano, A. Marx, and R. Gross, Nat. Phys. **6**, 772 (2010).
[19] P. Forn-Díaz, J. Lisenfeld, D. Marcos, J. J. García-Ripoll, E. Solano, C. J. P. M. Harmans, and J. E. Mooij, Phys. Rev. Lett. **105**, 237001 (2010).
[20] T. Schwartz, J. A. Hutchison, C. Genet,, and T. W. Ebbesen, Phys. Rev. Lett. **106**, 196405 (2011).
[21] Q. Zhang, M. Lou, X. Li, J. L. Reno, W. Pan, J. D. Watson, M. J. Manfra, and J. Kono, Nat. Phys. **12**, 1005 (2016).
[22] J. George, T. Chervy, A. Shalabney, E. Devaux, H. Hiura, C. Genet, and T. W. Ebbesen, Phys. Rev. Lett. **117**, 153601 (2016).
[23] F. Yoshihara, T. Fuse, S. Ashhab, K. Kakuyanagi, S. Saito, and K. Semba, Nat. Phys. **13**, 44 (2017).
[24] P. Forn-Díaz, J. García-Ripoll, B. Peropadre, J.-L. Orgiazzi, M. Yurtalan, R. Belyansky, C. Wilson, and A. Lupascu, Nat. Phys. **13**, 39 (2017).
[25] A. Bayer, M. Pozimski, S. Schambeck, D. Schuh, R. Huber, D. Bougeard, and C. Lange, Nano Lett. **17**, 6340 (2017).
[26] J. Braumüller, M. Marthaler, A. Schneider, A. Stehli, H. Rotzinger, M. Weides, and A. V. Ustinov, Nat. Commun. **8**, 779 (2017).
[27] N. K. Langford, R. Sagastizabal, M. Kounalakis, C. Dickel, A. Bruno, F. Luthi, D. J. Thoen, A. Endo, and L. DiCarlo, Nat. Commun. **8**, 1715 (2017).
[28] D. Lv, S. An, Z. Liu, J.-N. Zhang, J. S. Pedernales, L. Lamata, E. Solano, and K. Kim, Phys. Rev. X **8**, 021027 (2018).
[29] Y. Meng, A. Dareau, P. Schneeweiss, and A. Rauschenbeutel, Phys. Rev. X **8**, 031054 (2018).
[30] See Supplemental Material at http://link.aps.org/supplemental/10.1103/PhysRevLett.121.253603 for additional information on the experimental setup, models for numerical simulations, and a detailed derivation of the spin-motion coupling, which includes Refs. [31–34].
[31] E. Vetsch, D. Reitz, G. Sagué, R. Schmidt, S. T. Dawkins, and A. Rauschenbeutel, Phys. Rev. Lett. **104**, 203603 (2010).
[32] N. Schlosser, G. Reymond, and P. Grangier, Phys. Rev. Lett. **89**, 023005 (2002).
[33] J. R. Johansson, P. D. Nation, and F. Nori, Comput. Phys. Commun. **184**, 1234 (2013).
[34] M. Gangl and H. Ritsch, J. Phys. B **35**, 4565 (2002).
[35] B. Albrecht, Y. Meng, C. Clausen, A. Dareau, P. Schneeweiss, and A. Rauschenbeutel, Phys. Rev. A **94**, 061401 (2016).
[36] C. Cohen-Tannoudji and J. Dupont-Roc, Phys. Rev. A **5**, 968 (1972).
[37] P. S. Jessen, C. Gerz, P. D. Lett, W. D. Phillips, S. L. Rolston, R. J. C. Spreeuw, and C. I. Westbrook, Phys. Rev. Lett. **69**, 49 (1992).
[38] R. Mitsch, C. Sayrin, B. Albrecht, P. Schneeweiss, and A. Rauschenbeutel, Nat. Commun. **5**, 5713 (2014).
[39] Here, we choose the g_i/ω_i ratio as a figure of merit for USC. Another common choice consists in using the Ω_i/ω_i ratio [15,17,20,22], which would yield, in our case, $\Omega_y/\omega_y = 0.38(1)$ and $\Omega_x/\omega_x = 0.24(1)$.
[40] B. Arora, M. S. Safronova, and C. W. Clark, Phys. Rev. A **84**, 043401 (2011).
[41] I. Bloch, Nat. Phys. **1**, 23 (2005).
[42] A. M. Kaufman, B. J. Lester, and C. A. Regal, Phys. Rev. X **2**, 041014 (2012).

[43] J. D. Thompson, T. G. Tiecke, A. S. Zibrov, V. Vuletić, and M. D. Lukin, Phys. Rev. Lett. **110**, 133001 (2013).
[44] P. Schneeweiss, A. Dareau, and C. Sayrin, Phys. Rev. A **98**, 021801 (2018).
[45] M. Morinaga, I. Bouchoule, J.-C. Karam, and C. Salomon, Phys. Rev. Lett. **83**, 4037 (1999).
[46] N. Belmechri, L. Foerster, W. Alt, A. Widera, D. Meschede, and A. Alberti, J. Phys. B **46**, 104006 (2013).
[47] F. Vewinger, M. Heinz, R. Garcia Fernandez, N. V. Vitanov, and K. Bergmann, Phys. Rev. Lett. **91**, 213001 (2003).
[48] A. Smith, C. A. Riofrío, B. E. Anderson, H. Sosa-Martinez, I. H. Deutsch, and P. S. Jessen, Phys. Rev. A **87**, 030102 (2013).
[49] S. De Liberato, C. Ciuti,, and I. Carusotto, Phys. Rev. Lett. **98**, 103602 (2007).
[50] F. Beaudoin, J. M. Gambetta, and A. Blais, Phys. Rev. A **84**, 043832 (2011).